Quantum critical local spin dynamics near the Mott metal-insulator transition in infinite dimensions

Nagamalleswararao Dasari,[1,*] N. S. Vidhyadhiraja,[1] Mark Jarrell,[2,3] and Ross H. McKenzie[4,†]

[1]*Theoretical Sciences Unit, Jawaharlal Nehru Centre for Advanced Scientific Research, Jakkur, Bangalore 560064, India*

[2]*Department of Physics & Astronomy, Louisiana State University, Baton Rouge, Louisiana 70803, USA*

[3]*Center for Computation & Technology, Louisiana State University, Baton Rouge, Louisiana 70803, USA*

[4]*School of Mathematics and Physics, University of Queensland, Brisbane 4072, Australia*

Finding microscopic models for metallic states that exhibit quantum critical properties is a major theoretical challenge. We calculate the dynamical local spin susceptibility $\chi(T,\omega)$ for a Hubbard model at half-filling using dynamical mean-field theory, which is exact in infinite dimensions. Qualitatively distinct behavior is found in the different regions of the phase diagram: Mott insulator, Fermi liquid metal, bad metal, and a quantum critical region above the finite-temperature critical point. The signature of the latter is ω/T scaling, where ω is the frequency and T is the temperature. Our results are consistent with previous results showing scaling of the dc electrical conductivity, and they are relevant to experiments on organic charge-transfer salts.

I. INTRODUCTION

A wide range of materials exhibit properties characteristic of strongly correlated electrons. Materials include transition-metal oxides [1], cuprates [2], iron-based superconductors [3], heavy fermion compounds [4], and organic charge-transfer salts [5]. They exhibit emergent quantum states of matter such as unconventional superconductors, spin liquids, and non-Fermi-liquid metals. A major challenge is to understand these metallic states, which have properties quite distinct from those of simple elemental metals that can be described by Landau Fermi liquid theory. These unusual metallic states occur in close proximity to a Mott insulating phase [1] and/or to a quantum critical point [4]. The concept of quantum criticality may be a useful organizing principle [6–8].

The Hubbard model is one of the mostly widely studied effective Hamiltonians for strongly correlated electron systems. At the level of dynamical mean-field theory (DMFT) [9–14], at half-filling and zero temperature there is a first-order phase transition between metallic and Mott insulating phases as the interaction strength U is increased. Near half-filling, using the noncrossing approximation and quantum Monte Carlo, Pruschke *et al.* identified a region of anomalous transport [13,15]. It is characterized by linear-in-temperature resistivity, which corresponds to ω/T scaling, at high temperatures, crossing over to a Fermi liquid at lower T. The crossover scale between these regimes vanishes as half-filling is approached, and the slope of the linear-in-T resistivity varies like $1/x$, where x is the doping. More recently, Dobrosavljevic *et al.* identified a broad region of the T-U phase diagram displaying ω/T scaling in the half-filled model. They associated this behavior with a quantum critical point [16–18]. Furthermore, similar scaling was found in experimental data for three different organic charge-transfer salts that exhibit a critical point for the Mott transition in the temperature-pressure phase diagram [19]. In this paper, we show that the local spin dynamics of the

Hubbard model calculated with DMFT exhibits ω/T scaling that is characteristic of quantum criticality.

Quantum criticality and ω/T scaling

Varma *et al.* [20,21] showed that many of the anomalous properties of the metallic phase of cuprate superconductors at optimal doping can be described as a marginal Fermi liquid with a spin fluctuation spectrum that exhibits ω/T scaling. Finding concrete realistic theoretical microscopic fermion models that exhibit such scaling has proven challenging. Simulations of the two-dimensional Hubbard model reveal a quantum critical point at finite doping below a fan-shaped region of marginal Fermi liquid character in the self-energy [22,23]. There are several reviews of quantum criticality [6,8,24–29]. Sachdev has reviewed several spin and boson models [6] that exhibit ω/T scaling in the quantum critical region, associated with a quantum critical point. In such systems, the temperature itself is the relevant low-energy scale, rather than any scale in the model. For example, for the transverse field Ising model in one dimension (p. 73 of Ref. [6]), the spin dephasing rate $\Gamma = 0.4T$. For the two-dimensional $O(N \geqslant 3)$ rotor model in the large-N limit, $\Gamma = 0.94T/N$ (p. 142 of Ref. [6]). Parcollet and Georges [30] considered a particular limit of a random Heisenberg model that had a spin liquid ground state, and the dynamical spin susceptibility $\chi''(T,\omega)$ exhibited a form consistent with that conjectured in the marginal Fermi liquid scenario. Neutron scattering measurements found that the dynamic spin susceptibility exhibits ω/T scaling for an insulating antiferromagnetic spin-chain compound [31] and a kagomé lattice material [32]. Quantum criticality has been found for a Kondo boson-fermion model [33,34], motivated by ω/T scaling seen in neutron scattering experiments on several heavy fermion metals [4,35]. Specifically, inelastic neutron scattering gives the following ω/T scaling, for the wave-vector-dependent susceptibility, $\chi''(\omega,\vec{q})^{-1} = T^a F(\omega/T) + \chi'(\omega = 0,\vec{q})^{-1}$, where $\vec{q}$ is the wave vector and the exponent $a = 0.75$.

Our results are summarized in the phase diagram shown in Fig. 1. This diagram is deduced from the dynamical local spin susceptibility and is similar to that previously found

*nagamalleswararao.d@gmail.com
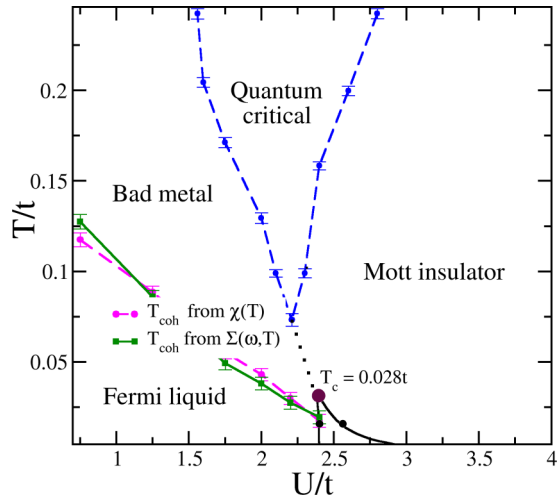
†r.mckenzie@uq.edu.au; condensedconcepts.blogspot.com

FIG. 1. Phase diagram determined from the dynamical spin susceptibility. In the quantum critical region, $\chi''(\omega)$ exhibits ω/T scaling with a spin relaxation rate that is proportional to the temperature. There is a finite-temperature critical point for the Mott metal-insulator transition ($T_c = 0.028t$). In the Mott insulating phase, $\chi''(T,\omega)/\omega$ tends to a δ-function peak as the temperature tends to zero. In the Fermi liquid phase, the spin relaxation rate is independent of temperature. The coherence temperature for the Fermi liquid was defined in two independent ways. The first is where the static spin susceptibility becomes temperature-dependent, and the second is where the imaginary part of the one-electron self-energy $\Sigma''(\omega = 0, T)$ deviates from a T^2 dependence (see Fig. 9 in the Appendix). The black lines define the coexistence region of the metal and Mott insulator, and the critical point, as determined in Ref. [37]. The black circles are our results. The blue symbols are the boundary of the quantum critical regime determined by the electron spin relaxation rate plotted in Fig. 2.

from scaling of the dc electrical conductivity near the critical point for the metal-insulator transition in the half-filled model [16,17]. Specifically, there is a quantum critical regime above the critical point; the signature is that the dynamical local spin susceptibility exhibits ω/T scaling. The local spin relaxation rate is linear in temperature, with a value $\Gamma \simeq 0.4T$. The occurrence of quantum critical properties in both the spin and charge sectors is consistent with recent work showing they are strongly coupled near the Mott transition [36].

II. MODEL HAMILTONIAN

We study the single-band Hubbard model on the Bethe lattice in infinite dimensions and at half-filling:

$$H = -t \sum_{\langle i,j \rangle, \sigma} (c_{i,\sigma}^\dagger c_{j,\sigma} + \text{H.c.}) + U \sum_i n_{i\uparrow} n_{i\downarrow}. \quad (1)$$

It involves two parameters: t, the nearest-neighbor hopping integral; and U, the Coulomb repulsion energy for two electrons on the same lattice site. The noninteracting ($U = 0$) density of states is semicircular with a full bandwidth $W = 2t$. DMFT is used to calculate the properties of the model [14]. In the limit of infinite dimensions or of infinite lattice connectivity, DMFT is exact. We do not allow for symmetry breaking such as antiferromagnetism. Previously

it has been shown that the metallic and Mott insulating phases coexist in the range $U_{c1} < U < U_{c2}$, where $U_{c1} = 2.4t$ and $U_{c2} = 2.9t$ [37]. There is a finite-temperature critical point at $U_c = 2.4t$ and $T_c = 0.028t$. Our results at $\beta \equiv 1/T = 70/t$ are consistent with this earlier work (compare Fig. 1).

III. METHOD

The hybridization expansion version of the continuous-time quantum Monte Carlo (CTQMC) algorithm [38] is used as a DMFT impurity solver to calculate the spin dynamics at finite temperature. The main advantages of this method are that it is numerically exact and the fermionic sign problem does not occur until very low temperatures in the Fermi liquid regime. The vertex-corrected local spin susceptibility $\chi(\tau) \equiv \langle S_z(\tau) S_z(0) \rangle$ is computed at imaginary times and then Fourier-transformed to Matsubara frequencies.

In CTQMC simulations, we accumulate adjacent imaginary-time one- and two-particle Green's-function data into equal bins [39]. This may be done efficiently, but the data obtained are correlated in both Monte Carlo and imaginary time and hence may be problematic for analytic continuation via the maximum entropy method [40,41]. By increasing the bin size, we reduce correlations between adjacent bin averages, ensuring that the binned data have a Gaussian distribution. We can quantify this by fitting the histogram of the binned data to a Gaussian form and by calculating the third and fourth moments of the histogram to ensure that they are very small ($\sim 10^{-1}$–10^{-2}). However, correlations between errors of the Green's function at adjacent time slices remain, and they are characterized by the off-diagonal elements of the covariance matrix (C). To remove these correlations, we diagonalize the covariance matrix with a unitary transformation U,

$$(U^{-1}CU)_{ij} = \sigma_i'^2 \delta_{ij}. \quad (2)$$

We then rotate the data (G) and kernel (K) into this diagonal representation $K' = U^{-1}K$, $G' = U^{-1}G$, where we may carry out the maximum entropy calculations on independent samples.

Empirically, Jarrell *et al.* [40] find that accurate calculations of the covariance require that the number of bins be chosen such that $N_{\text{bins}} \geqslant 2L$, where L is the number of required independent eigenvectors. In our calculations, we use $N_{\text{bins}} = 300$ and $L = 15$. We also perform calculations in the critical region by increasing the number of bins from 300 to 1000 to ensure robustness and observe that the relative change in spin-relaxation rate Γ is very marginal ($\sim 10^{-3}$). Hence, in this paper, we show data obtained for 300 bins.

As the default model for the analytic continuation, we use the closed analytical form results of Salomaa [42] for the resonant level model (Anderson single-impurity model with $U = 0$). Given the data, in the Salomaa model the parameter for the width of the spectral density is chosen such that it maximizes the posterior probability of the model [41]. We also calculate $\chi''(T,\omega)$ by using another default model provided by Bouadim *et al.* [43]. We find that our results are independent of the choice of default model, suggesting that the analytical continuation procedure is quite robust.

IV. SPIN RELAXATION RATE

From the dynamical local spin susceptibility, $\chi(T,\omega) \equiv \chi'(T,\omega) + i\chi''(T,\omega)$, a spin relaxation rate can be defined by

$$\Gamma(U,T) \equiv \lim_{\omega \to 0} \frac{\omega\chi'(T,\omega=0)}{\chi''(T,\omega)}. \quad (3)$$

This is similar to the (dephasing) relaxation rate defined by Sachdev for a spin model at the ordering wave vector (Ref. [6], p. 73). If $\chi(T,\omega)$ has a simple Lorentzian or Drude form, then Γ corresponds to the width of the peak at zero frequency in the spectral density, $\chi''(T,\omega)/\omega$. Our results for the temperature dependence of Γ are shown in Fig. 2.

On the metallic side of the Mott transition, the signature of the crossover from a Fermi liquid to a bad metal (with increasing temperature above T_{coh}) is that $\Gamma(T,U)$ decreases smoothly from a small T-independent value below T_{coh} to a temperature-dependent value. Above this temperature the spin dynamics is weakly damped, similar to the localized weakly interacting magnetic moments present in the Mott insulating phase. The latter was conjectured to be the character of the bad metallic state, based on the large entropy and static spin susceptibility found from finite-temperature Lanczos calculations for the Hubbard model on the triangular lattice at half-filling [44].

Recent DMFT calculations of charge-transport properties of a doped Hubbard model [45] identified the existence of well-defined quasiparticle-like excitations [resilient quasiparticles (RQPs)] well above the coherence temperature (T_{coh}) and their gradual extinction with the crossover to the bad metallic regime

(T_{MIR}) where the resistivity becomes comparable to the Mott-Ioffe-Regel limit. Our results suggest that the spin relaxation rate in the RQP regime behaves quite differently in comparison with the low-temperature Fermi liquid and high-temperature bad metallic regime. In fact, this might be relevant to the recently observed slowdown of the relaxation dynamics near the Mott transition in the quench dynamics of the Hubbard model [46]. Our results suggest the need to investigate spin dynamics in the doped case.

V. QUANTUM CRITICAL SCALING

Figure 3 shows that above the critical point $\chi''(T,\omega)$ exhibits ω/T scaling characteristic of quantum criticality, i.e., $\chi''(T,\omega) = \chi'(T,\omega=0)F(\omega/T)$. For low frequencies, the scaling function is best fit to a power law, $F(x) = 2.3x$. For $T \gtrsim 0.069t$, the scaling covers about three decades in the ratio ω/T. For comparison, in the metallic (Fig. 4) and Mott insulating (Fig. 5) regions such scaling clearly does not occur. In the Mott insulating phase, $\chi''(T,\omega)/\omega$ tends toward a δ-function peak, i.e., $\Gamma(T) \to 0$ as $T \to 0$ (compare Fig. 5). This reflects the decoupled local moments in the Mott phase. In DMFT there is no Heisenberg antiferromagnetic exchange interaction between localized spins on neighboring lattice sites. At zero temperature, the δ-function peak is also clearly seen in dynamic DMRG calculations [47].
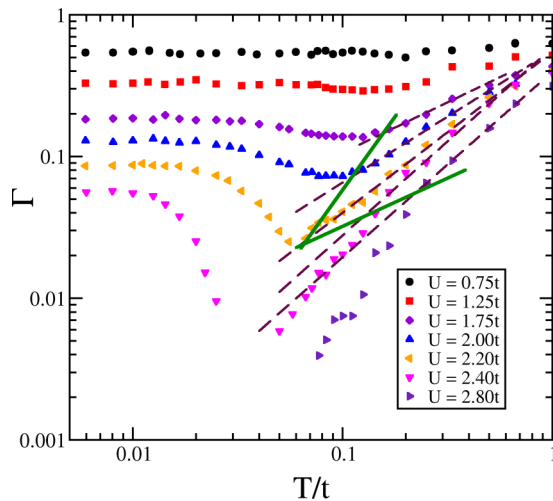

FIG. 2. Electron spin relaxation rate $\Gamma(U,T)$ as a function of temperature for different U values. In the Fermi-liquid regime of the metallic phase ($T < T_{\mathrm{coh}}$), the relaxation rate is nonzero and independent of temperature. This rate decreases by more than an order of magnitude as the Mott insulator is approached. Above the coherence temperature, Γ decreases with increasing temperature, reflecting the decreasing interaction between the spins of the electrons, which become more localized as the temperature increases. In the Mott insulator ($U > 2.4t$), the rate tends to zero as the temperature tends to zero, reflecting the decoupled local moments. In the quantum critical regime, the rate is a power law as a function of temperature. For $U = 2.2t$, the rate is approximately linear in temperature, $\Gamma \simeq 0.4T$. The green lines define the boundary of the quantum critical region in Fig. 1.
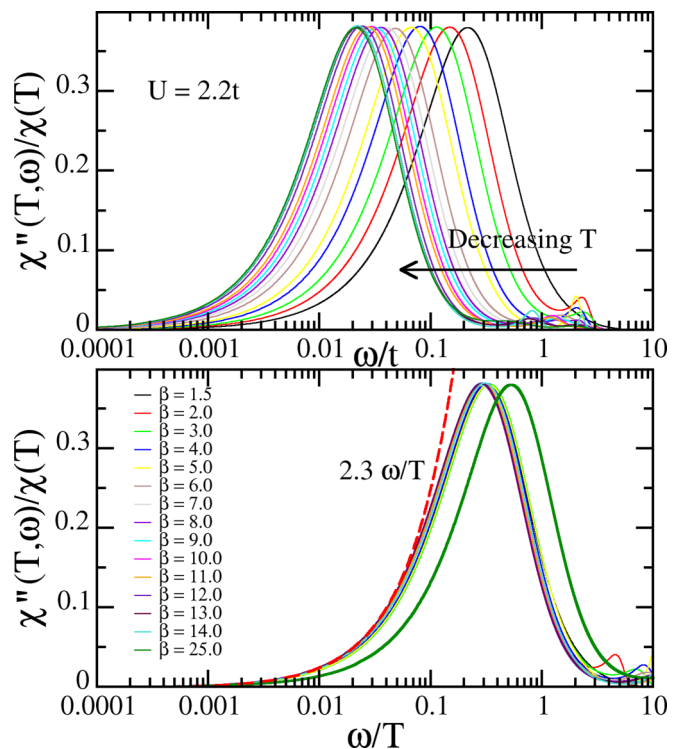

FIG. 3. Quantum critical scaling of the dynamical spin susceptibility near the Mott transition. The upper panel shows the frequency dependence of the imaginary part of the susceptibility for $U = 2.2t$ for a range of temperatures ($T = 1/\beta$). The lower panel shows the same data with the frequency scaled by temperature. Scaling occurs for all $T \gtrsim 0.069t$, but it fails for $T = 0.04t$ (green curve) consistent with the extent of the QC region in Fig. 1. The dashed line $2.3\omega/T$ is a best fit to the low-frequency data.
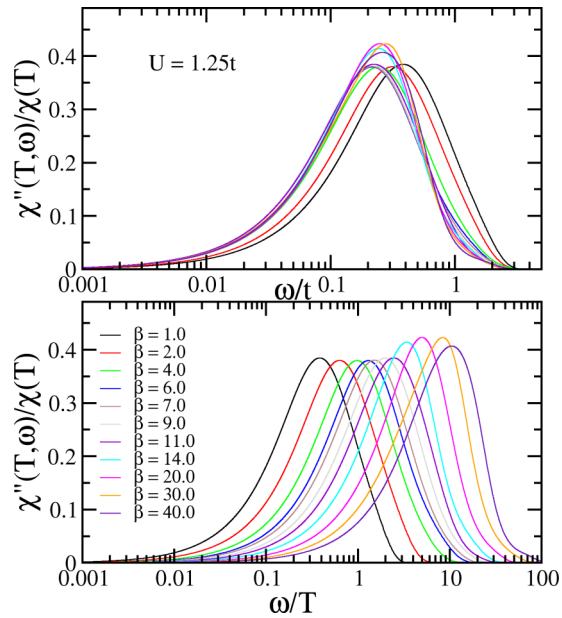
FIG. 4. Frequency dependence of the dynamical spin susceptibility in the metallic phase. The upper panel shows the frequency dependence of the imaginary part of the susceptibility for $U/t = 1.25$ for a range of temperatures and on a linear scale. The lower panel shows the same data on a log-log plot with the frequency scaled by temperature. Unlike in the quantum critical regime, ω/T scaling is not observed.
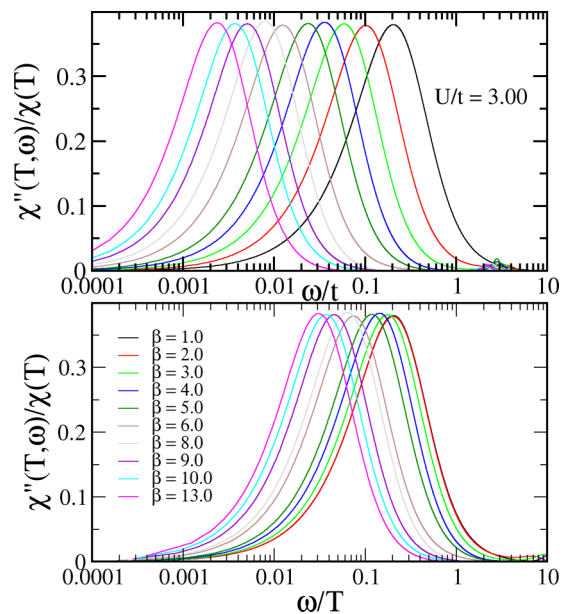

FIG. 5. Frequency dependence of the dynamical spin susceptibility in the Mott insulating phase. The upper panel shows the frequency dependence of the imaginary part of the susceptibility for $U/t = 3.0$ for a range of temperatures and on a linear scale. Note how as the temperature tends to zero, the peak width tends to zero and that one sees features around $\omega = U$, associated with the Hubbard bands. The lower panel shows the same data on a log-log plot with the frequency scaled by temperature. Unlike in the quantum critical regime, ω/T scaling is not observed.
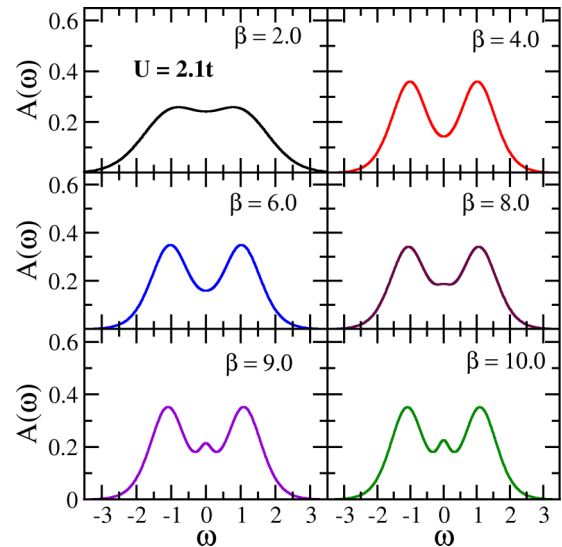

FIG. 6. One electron spectral density for $U/t = 2.10$ for different temperatures in the quantum critical region. Compare Fig. 7 in Ref. [17]. The absence of a quasiparticle peak at $\omega = 0$ is characteristic of a bad metal [48].

In Fig. 6 we show the one-electron spectral density for $U/t = 2.10$. It can be seen that for temperatures in the quantum critical region, there is an absence of the quasiparticle peak at ω that is characteristic of a Fermi liquid.

A. Boundary conformal field theory scaling

Scaling with ω/T is associated with the following scaling of the imaginary-time susceptibility:

$$\chi(\tau) \sim (\pi T / \sin(\pi\tau T))^{2\lambda}, \qquad (4)$$

where τ is the imaginary time [49]. It has been found that such scaling does hold for a Kondo boson-fermion model [33,34,50], a fractionalized Fermi liquid in a holographic metal [51], a pseudogap Anderson model [52], and the gapped single-impurity Anderson model [53]. We do not observe such scaling in $\chi(\tau)$, but we do observe it in the one-electron local Green's function $G(\tau)$ (compare Fig. 7). Our results illustrate that ω/T scaling does not necessarily imply the scaling characteristic of boundary conformal field theory (CFT).

VI. NMR PROPERTIES

The most direct experimental probe of the low-frequency behavior of the dynamical local spin susceptibility $\chi''(\omega)$ is through nuclear magnetic resonance (NMR). In contrast, neutron scattering measures the dynamical susceptibility at a finite wave vector.

Nuclear spin relaxation rate

This is given by

$$\frac{1}{T_1 T} = A^2 \lim_{\omega \to 0} \frac{\chi''(T,\omega)}{\omega} \qquad (5)$$

and in simple metals this quantity is independent of temperature (Korringa) (Ref. [54], p. 156). Note that there is
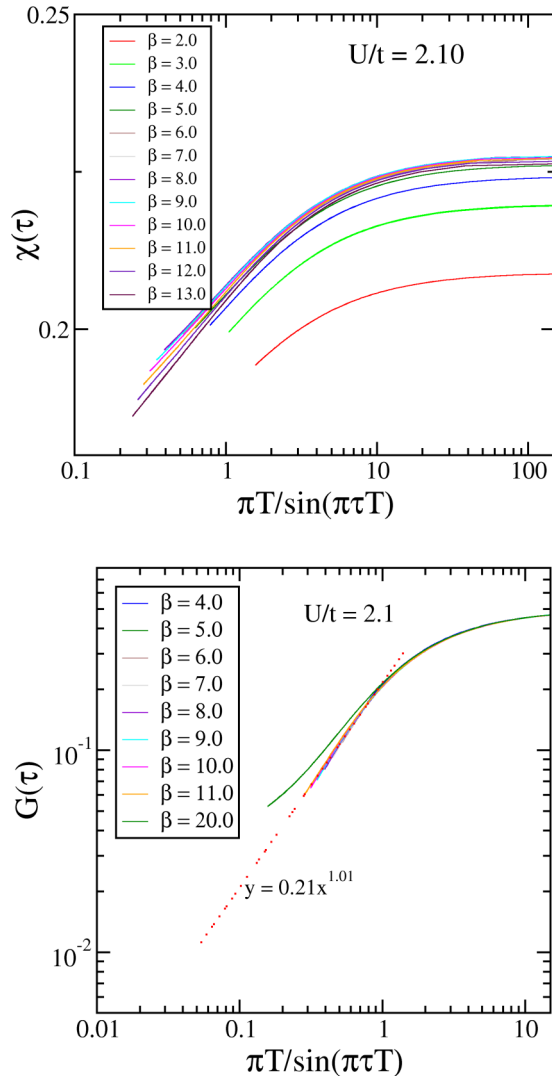
FIG. 7. The upper panel shows the failure of boundary conformal field theory scaling of the imaginary-time dependence of the susceptibility $\chi(\tau)$. The lower panel shows the boundary conformal field theory scaling of the imaginary-time dependence of the one-electron Green's function, $G(\tau)$. Curves are shown for $U = 2.10t$ and for a range of temperatures ($\beta = 1/T$). We tried to find a temperature-dependent rescaling parameter for the vertical axis such that all curves of this spin susceptibility collapse on top of each other. However, we did not find any such rescaling parameter.

a relationship to the electron spin relaxation rate Γ defined in Eq. (3), $T_1 \sim \Gamma/[T\chi'(T,\omega=0)]$. Hence, T_1 being independent of T, which is sometimes associated with quantum criticality [7,55], is not the same as Γ being linear in T, if the temperature dependence of the dc susceptibility is significant (as it is here). The top panel of Fig. 8 shows $1/(T_1 T)$ as a function of temperature for a range of U values. Below the coherence temperature for the metallic phase it is independent of temperature, as expected. Its magnitude is significantly enhanced as the Mott insulator is approached.

For comparison, we note that Zitko, Osolin, and Jeglic [56] calculated $\chi''(T,\omega)/\omega$ for a doped Hubbard model at filling $n = 0.8$ using the numerical normalization group as an impurity solver in DMFT. They found that $1/T_1$ was a
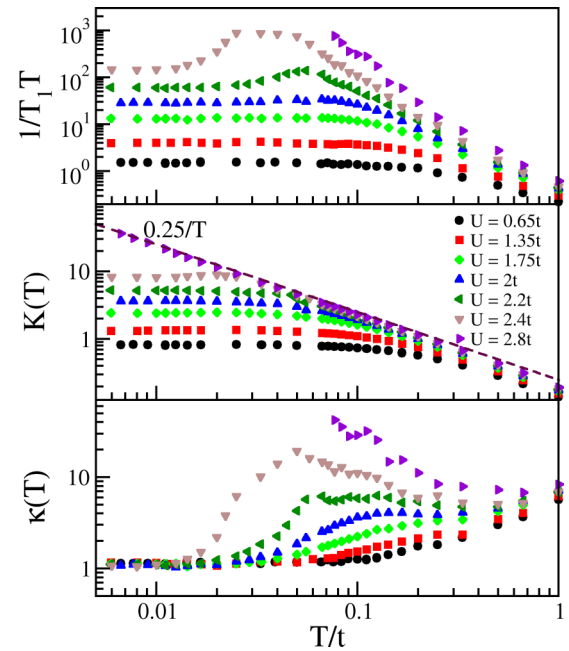

FIG. 8. Temperature dependence of NMR properties for a range of U values. The top panel shows the nuclear spin relaxation rate, $1/(T_1 T)$. The middle panel shows the local static susceptibility (Knight shift). Note that both quantities are significantly enhanced as the Mott transition is approached on the metallic site. Below the coherence temperature T_{coh}, both are independent of temperature, characteristic of a Fermi liquid. Well above T_{coh}, the static susceptibility approaches the Curie form [$\chi = 1/(4T)$, shown by the purple dashed line], suggesting unscreened local moments. The bottom panel shows the Korringa-Shiba ratio, defined in Eq. (6). Below T_{coh} it approaches 1, and above T_{coh} it is larger than 1 and increases with U.

nonmonotonic function of temperature and increased by up to two orders of magnitude as U/W increased from 0 to 4, and it was weakly temperature-dependent in the bad metal regime.

NMR Knight shift

In a lattice system, this is given by $K(T) = A\chi'(\vec{q}=0,\omega=0)$, where $\vec{q}$ is the wave vector and A is the hyperfine coupling. Note that the right-hand side is not the same quantity as the local spin susceptibility, $\chi'(\omega=0) \equiv \sum_{\vec{q}} \chi'(\vec{q},\omega=0)$, that is our focus here. Nevertheless, for reasons of simplicity, we do not consider this difference here. The middle panel of Fig. 8 shows the static local susceptibility as a function of temperature for a range of U values. Here we work with units such that $A = 1$. Note that in the metallic phase as the temperature increases there is a crossover from a temperature-independent value at low temperatures, characteristic of a Fermi liquid, to a Curie form $1/(4T)$, characteristic of localized noninteracting spins.

Korringa-Shiba relation

In a simple Fermi liquid, the following dimensionless ratio is unity in the absence of vertex corrections [57],

$$\kappa(T) \equiv \lim_{\omega \to 0} \frac{\chi''(T,\omega)}{2\pi\omega\chi'(T,\omega)^2}. \tag{6}$$

Shiba [58] showed that for the single Anderson impurity model, $\kappa(T) = 1$ in the Kondo regime. Values of κ larger and less than 1 are often associated, respectively, with antiferromagnetic and ferromagnetic fluctuations [57]. In Fig. 8 we plot this ratio as a function of temperature for a range of U, and we find that it can be much larger than unity and increases as the Mott insulating phase is approached from the metallic side. However, in the Fermi liquid regime, κ is close to 1.

VII. RELEVANCE TO EXPERIMENTAL RESULTS FOR ORGANIC CHARGE-TRANSFER SALTS

The materials that are arguably closest to the model considered here are organic charge-transfer salts, e.g., κ-(BEDT-TTF)$_2 X$. They can be modeled in terms of an effective Hamiltonian that is a single-band Hubbard model on an anisotropic triangular lattice at half-filling [5]. As the pressure increases, these materials undergo a first-order phase transition from a Mott insulator to a Fermi liquid metal. It has been found that DMFT describes the crossover from a coherent Fermi liquid to a bad metallic state with increasing temperature [48]. Furthermore, DMFT gives a quantitative description of the resistivity [59] and the frequency-dependent optical conductivity [60] for these organics. Near the critical point, some signatures of critical behavior have been reported in the conductivity [19,61] and NMR [62]. For a diverse set of κ-(BEDT-TTF)$_2 X$ above some temperature of the order $T_b \sim 50$ K, the NMR relaxation rate becomes roughly independent of temperature [63]. Broadly, this is consistent with the quantum criticality discussed here. On the other hand, there are alternative explanations in terms of short-range antiferromagnetic spin fluctuations [63], and the experiments cover a relatively narrow temperature range, roughly 50–300 K, which is not even a single decade. Our results compare well qualitatively with experimental results for κ-(BEDT-TTF)$_2$Ag(CN)$_3$ [see Fig. 3(a) in Ref. [64]] and κ-(BEDT-TTF)$_4$Hg$_{2.89}$Br$_8$ [see Fig. 3(c) in Ref. [65]]. (It should be noted, however, that the latter material has been suggested to be doped away from half-filling.) As the pressure increases, $1/(T_1 T)$ decreases by more than an order of magnitude. It smoothly crosses over from a form that is monotonically decreasing with temperature above about 10 K at low pressures to a weak temperature dependence (Korringa) at higher pressures. In several organics, the Korringa ratio is observed to be temperature-dependent with large values of order 10 [66,67]. We hope our results will stimulate new experiments.

VIII. DISCUSSION AND CONCLUSIONS

The observed quantum critical scaling in the dynamical spin susceptibility above T_c is what one expects to be associated with a zero-temperature quantum critical point [17,68]. This quantum critical region might be extended down to zero temperature by varying some parameter such as doping. For example, the crossover scale between the region of linear resistivity and the low-temperature Fermi liquid regime was found to vanish as half-filling is approached [13,15] (compare Fig. 9 in Ref. [17]). Recent exact results on doped Mott insulators within DMFT [68] identified a continuous quantum phase transition from the metal to Mott insulator phase
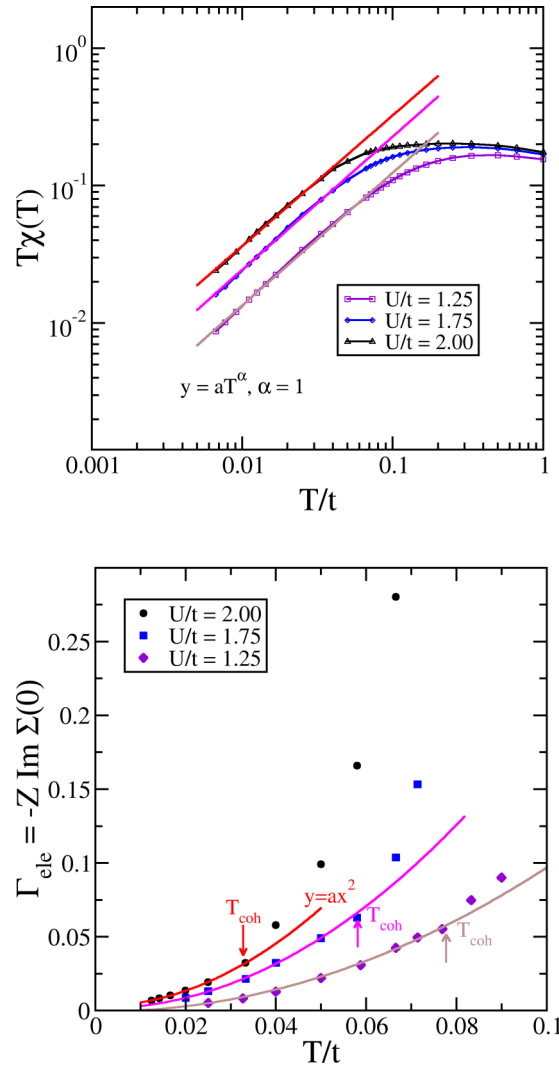

FIG. 9. Determination of the Fermi liquid coherence temperature. Upper panel: from the static local spin susceptibility, $T_{\rm coh}$ is defined as the temperature at which $\chi(T)$ deviates from the temperature independence characteristic of a Fermi liquid. Lower panel: from the self-energy for the one-electron Green's function, $T_{\rm coh}$ is defined as the temperature at which $Z\Sigma''(\omega = 0, T)$ deviates from the quadratic temperature dependence characteristic of a Fermi liquid.

through the absence of a coexistence region in the limit of particle-hole asymmetry parameter $1 - \frac{2\mu}{U} \to 1$. This implies that the bottom of the quantum critical fan associated with Mott quantum criticality can be pushed down to zero temperature in this limit. CTQMC results from Vucicevic *et al.* [18] on the doped Mott insulator indeed support such an implication, since they show that the quantum critical scaling of the dc conductivity extends to much lower temperatures than what was found in the symmetric case.

Quantum criticality means that other dynamical response functions such as the frequency-dependent conductivity should also exhibit ω/T scaling. We observed that in the quantum critical region, the one-particle Green's function exhibits ω/T scaling and hence one could expect the same scaling for the optical conductivity in the critical region since only the zeroth-order bubble survives in the infinite-dimensional limit.

The nature of the quantum critical point is also of interest. In strongly correlated electronic systems, two types of quantum criticality are most often discussed [28,29]: a local quantum critical point associated with the destruction of Kondo screening [28], and a Moriya-Hertz-Millis (see, e.g., Ref. [27]) critical point associated with the destruction of a spin-density wave or some other ordered phase. These two scenarios for electron models may be distinguished by the fact that the point where the Kondo screening vanishes at zero temperature coincides with the QCP in the local model, but not in the Moriya-Hertz-Millis scenario. In addition, the former displays ω/T scaling in the quantum critical region, whereas the latter displays $(\omega/T)^{1-\theta}$ scaling with $\theta > 0$ [28]. As noted previously [13,15], the crossover scale between the region of anomalous transport, linear resistivity, and the Fermi liquid vanishes as the doping $x \to 0$, and the slope of the linear in temperature resistivity varies like $1/x$, both strongly suggesting that the QCP is at half-filling (but not necessarily at zero chemical potential, since it varies discontinuously with the opening of the Mott gap). These phenomena coincide with a vanishing Kondo peak in the density of states, with width given by the crossover scale, as $x \to 0$. Our findings, together with these previous results, indicate that the QCP in this model is a local quantum critical point.

It is interesting to speculate if the quantum criticality found here could be related to the quantum critical point (QCP) found at finite doping in the 2D Hubbard model using dynamical cluster QMC simulations [22,23]. There the QCP separates the pseudogap and Fermi liquid regions, with a large region of ω/T marginal Fermi liquid [20] scaling above the QCP. Calculations are now underway to explore this possibility.

In summary, the main significance of this work is that it gives a concrete example of a fermion model that has a metallic state in proximity to a Mott insulating state and has dynamical local spin fluctuations that exhibit the ω/T scaling that is characteristic of local quantum criticality.

APPENDIX: DETERMINATION OF THE COHERENCE TEMPERATURE

Figure 9 shows the Fermi liquid coherence temperature determined by two distinct methods. This is not necessarily the same for different properties. Sometimes, it is smaller for two-particle properties than for single-particle ones [72]. For example, in the Kondo problem the Kondo resonance exists up to temperatures of $2T_K$, while the spin susceptibility saturates to a Pauli form only below $T = 0.2T_K$. For example, in Ref. [73] compare Figs. 2, 7, and 16, which show the specific heat, spectral density, and thermopower, respectively.

[1] M. Imada, A. Fujimori, and Y. Tokura, Rev. Mod. Phys. **70**, 1039 (1998).

[2] B. Keimer, S. Kivelson, M. Norman, S. Uchida, and J. Zaanen, Nature (London) **518**, 179 (2015).

[3] J. G. Analytis, H.-H. Kuo, R. D. McDonald, M. Wartenbe, P. M. C. Rourke, N. E. Hussey, and I. R. Fisher, Nat. Phys. **10**, 194 (2014).

[4] P. Gegenwart, Q. Si, and F. Steglich, Nat. Phys. **4**, 186 (2008).

[5] B. J. Powell and R. H. McKenzie, Rep. Prog. Phys. **74**, 056501 (2011).

[6] S. Sachdev, *Quantum Phase Transitions*, 1st ed. (Cambridge University Press, Cambridge, 1999).

[7] S. Sachdev, Science **288**, 475 (2000).

[8] S. Sachdev and B. Keimer, Phys. Today **64**(2), 29 (2011).

[9] W. Metzner and D. Vollhardt, Phys. Rev. Lett. **62**, 324 (1989).

[10] V. Janiš, Z. Phys. B **83**, 227 (1991).

[11] A. Georges and G. Kotliar, Phys. Rev. B **45**, 6479 (1992).

[12] M. Jarrell, Phys. Rev. Lett. **69**, 168 (1992).

[13] T. Pruschke, M. Jarrell, and J. Freericks, Adv. Phys. **44**, 187 (1995).

[14] A. Georges, G. Kotliar, W. Krauth, and M. J. Rozenberg, Rev. Mod. Phys. **68**, 13 (1996).

[15] M. Jarrell and T. Pruschke, Phys. Rev. B **49**, 1458 (1994).

[16] H. Terletska, J. Vučičević, D. Tanasković, and V. Dobrosavljević, Phys. Rev. Lett. **107**, 026401 (2011).

[17] J. Vučičević, H. Terletska, D. Tanasković, and V. Dobrosavljević, Phys. Rev. B **88**, 075143 (2013).

[18] J. Vučičević, D. Tanasković, M. J. Rozenberg, and V. Dobrosavljević, Phys. Rev. Lett. **114**, 246402 (2015).

[19] T. Furukawa, K. Miyagawa, H. Taniguchi, R. Kato, and K. Kanoda, Nat. Phys. **11**, 221 (2015).

[20] C. M. Varma, P. B. Littlewood, S. Schmitt-Rink, E. Abrahams, and A. E. Ruckenstein, Phys. Rev. Lett. **63**, 1996 (1989).

[21] C. M. Varma, Rep. Prog. Phys. **79**, 082501 (2016).

[22] N. S. Vidhyadhiraja, A. Macridin, C. Sen, M. Jarrell, and M. Ma, Phys. Rev. Lett. **102**, 206407 (2009).

[23] E. Khatami, K. Mikelsons, D. Galanakis, A. Macridin, J. Moreno, R. T. Scalettar, and M. Jarrell, Phys. Rev. B **81**, 201101 (2010).

[24] M. Vojta, Rep. Prog. Phys. **66**, 2069 (2003).

[25] D. Belitz, T. R. Kirkpatrick, and T. Vojta, Rev. Mod. Phys. **77**, 579 (2005).

[26] P. Coleman and A. J. Schofield, Nature (London) **433**, 226 (2005).

[27] H. v. Löhneysen, A. Rosch, M. Vojta, and P. Wölfle, Rev. Mod. Phys. **79**, 1015 (2007).

[28] Q. Si, Quantum Criticality and the Kondo Lattice, in *Understanding Quantum Phase Transitions*, edited by L. Carr (CRC, Boca Raton, FL, 2010), pp. 193–216.

[29] Q. Si, J. H. Pixley, E. Nica, S. J. Yamamoto, P. Goswami, R. Yu, and S. Kirchner, J. Phys. Soc. Jpn. **83**, 061005 (2014).

[30] O. Parcollet and A. Georges, Phys. Rev. B **59**, 5341 (1999).

[31] B. Lake, D. A. Tennant, C. D. Frost, and S. E. Nagler, Nat. Mater. **4**, 329 (2005).

[32] J. S. Helton, K. Matan, M. P. Shores, E. A. Nytko, B. M. Bartlett, Y. Qiu, D. G. Nocera, and Y. S. Lee, Phys. Rev. Lett. **104**, 147201 (2010).

[33] L. Zhu, S. Kirchner, Q. Si, and A. Georges, Phys. Rev. Lett. **93**, 267201 (2004).

[34] S. Kirchner and Q. Si, Phys. Rev. Lett. **100**, 026403 (2008).

[35] A. Schröder, G. Aeppli, R. Coldea, M. Adams, O. Stockert, H. Löhneysen, E. Bucher, R. Ramazashvili, and P. Coleman, Nature (London) **407**, 351 (2000).

[36] T.-H. Lee, S. Florens, and V. Dobrosavljević, Phys. Rev. Lett. **117**, 136601 (2016).

[37] P. Werner and A. J. Millis, Phys. Rev. B **75**, 085108 (2007).

[38] E. Gull, A. J. Millis, A. I. Lichtenstein, A. N. Rubtsov, M. Troyer, and P. Werner, Rev. Mod. Phys. **83**, 349 (2011).

[39] E. Gull, H. Hafermann, and P. Werner, Documentation–Hybridization Expansion CT-QMC solver version 3.0b1.

[40] M. Jarrell and J. E. Gubernatis, Phys. Rep. **269**, 133 (1996).

[41] M. Jarrell, J. E. Gubernatis, and R. N. Silver, Phys. Rev. B **44**, 5347 (1991).

[42] M. Salomaa, Z. Phys. B **25**, 49 (1976).

[43] K. Bouadim, Y. L. Loh, M. Randeria, and N. Trivedi, Nat. Phys. **7**, 884 (2011).

[44] J. Kokalj and R. H. McKenzie, Phys. Rev. Lett. **110**, 206402 (2013).

[45] X. Deng, J. Mravlje, R. Žitko, M. Ferrero, G. Kotliar, and A. Georges, Phys. Rev. Lett. **110**, 086401 (2013).

[46] S. Sayyad and M. Eckstein, Phys. Rev. Lett. **117**, 096403 (2016).

[47] C. Raas and G. S. Uhrig, Phys. Rev. B **79**, 115136 (2009).

[48] J. Merino and R. H. McKenzie, Phys. Rev. B **61**, 7996 (2000).

[49] I. Affleck, Acta Phys. Polon. B **26**, 1869 (1995).

[50] M. T. Glossop, S. Kirchner, J. H. Pixley, and Q. Si, Phys. Rev. Lett. **107**, 076404 (2011).

[51] S. Sachdev, Phys. Rev. Lett. **105**, 151602 (2010).

[52] J. H. Pixley, S. Kirchner, K. Ingersent, and Q. Si, Phys. Rev. B **88**, 245111 (2013).

[53] N. Dasari, S. Acharya, A. Taraphder, J. Moreno, M. Jarrell, and N. Vidhyadhiraja, arXiv:1509.09163.

[54] C. P. Slichter, *Principles of Magnetic Resonance*, 3rd ed. (Springer, Berlin, 1996).

[55] K. Kitagawa, K. Ishida, R. S. Perry, T. Tayama, T. Sakakibara, and Y. Maeno, Phys. Rev. Lett. **95**, 127001 (2005).

[56] R. Zitko, Z. Osolin, and P. Jeglic, Phys. Rev. B **91**, 155111 (2015).

[57] E. Yusuf, B. J. Powell, and R. H. McKenzie, J. Phys.: Condens. Matter **21**, 195601 (2009).

[58] H. Shiba, Prog. Theor. Phys. **54**, 967 (1975).

[59] P. Limelette, P. Wzietek, S. Florens, A. Georges, T. A. Costi, C. Pasquier, D. Jérome, C. Mézière, and P. Batail, Phys. Rev. Lett. **91**, 016401 (2003).

[60] J. Merino, M. Dumm, N. Drichko, M. Dressel, and R. H. McKenzie, Phys. Rev. Lett. **100**, 086404 (2008).

[61] F. Kagawa, K. Miyagawa, and K. Kanoda, Nature (London) **436**, 534 (2005).

[62] F. Kagawa, K. Miyagawa, and K. Kanoda, Nat. Phys. **5**, 880 (2009).

[63] B. J. Powell, E. Yusuf, and R. H. McKenzie, Phys. Rev. B **80**, 054505 (2009).

[64] Y. Shimizu, T. Hiramatsu, M. Maesato, A. Otsuka, H. Yamochi, A. Ono, M. Itoh, M. Yoshida, M. Takigawa, Y. Yoshida, and G. Saito, Phys. Rev. Lett. **117**, 107203 (2016).

[65] Y. Eto, M. Itaya, and A. Kawamoto, Phys. Rev. B **81**, 212503 (2010).

[66] S. M. De Soto, C. P. Slichter, A. M. Kini, H.-H. Wang, U. Geiser, and J. M. Williams, Phys. Rev. B **52**, 10364 (1995).

[67] M. Itaya, Y. Eto, A. Kawamoto, and H. Taniguchi, Phys. Rev. Lett. **102**, 227003 (2009).

[68] D. E. Logan and M. R. Galpin, J. Phys.: Condens. Matter **28**, 025601 (2016).

[69] H. H. Hafermann, P. Werner, and E. Gull, Comput. Phys. Commun. **184**, 1280 (2013).

[70] P. Werner, A. Comanac, L. de' Medici, M. Troyer, and A. J. Millis, Phys. Rev. Lett. **97**, 076405 (2006).

[71] B. Bauer *et al.*, J. Stat. Mech.: Theor. Exp. (2011) P05001.

[72] J. Mravlje, M. Aichhorn, T. Miyake, K. Haule, G. Kotliar, and A. Georges, Phys. Rev. Lett. **106**, 096401 (2011).

[73] T. Costi, A. Hewson, and V. Zlatic, J. Phys.: Condens. Matter **6**, 2519 (1994).